Mineralogical and geochemical investigations of the Middle Eocene ironstones, El Bahariya Depression, Western Desert, Egypt.

[a*] W. Salama (swalid@sci.cu.edu.eg), [a] M. M. El Aref (elaref2000@yahoo.com), [b] R. Gaupp (reinhard.gaupp@uni-jena.de)

[a] Geology Department, Faculty of Science, Cairo University, Giza-12613, Egypt.
[b] Institute of Earth Sciences, Friedrich Schiller University Jena, Germany.

Abstract

The Middle Eocene ironstone succession is located in the northeastern part of El Bahariya Depression, Western Desert, Egypt. This succession is subdivided into lower and upper sequences and consists of two main shallow marine ironstone facies associations. The first is a lagoonal manganiferous mud and fossiliferous ironstone facies association and consists mainly of goethite and hematite, detrital minerals (quartz, rutile, and feldspars), manganese minerals (todorokite, psilomelane, pyrolusite, birnessite, aurorite and manjiroite), and authigenic clay minerals (kaolinite and illite). The second is a peritidal microbially mediated stromatolitic and nummulitic-ooidal-oncoidal ironstone facies association and consists of goethite, apatite, and secondary minerals that include quartz, jarosite, psilomelane, and pyrolusite. Organic materials such as proteinaceous compounds, lipids, cellulose, and carotenoids were detected in the cortices of the ferruginous ooids and oncoids. The marine ironstone facies were exposed to subaerial weathering and subsurface alteration processes. The weathering resulted in the formation of lateritic iron ores and paleosols during humid climatic periods. The lateritic iron ores consist mainly of colloform goethite, hematite and psilomelane. The identification of cavity-filling sulfate, nitrate, carbonate and silicate minerals in the marine ironstones and the lateritic iron ore may indicate more recent alteration under arid climatic conditions. The subsurface alteration is attributed to the oxidation of sulfides, primarily pyrite, and weathering of glauconitic clastic rocks in the underlying Cenomanian Bahariya Formation during the interaction with acidic heated groundwater. The formation of ferrous and ferric sulfate, and silicate minerals, and mobilization of trace metals are the products of the alteration process. Enrichments in Ba, Co, K,

1

Pb and Sr are correlated with manganese oxides, whereas anomalous P, V, Cr, Ni, Zn, As, Mo, and U are correlated with iron oxyhydroxides.

Keywords: Mineralogy, geochemistry, ironstone, El Bahariya Depression, Egypt

Corresponding author:

Walid Salama

*Present address: Geology Department, Faculty of Science, Cairo University Giza-12613, Egypt.

Tel: 002119746746, Fax: 0020235727556, E-mail: walidsamir@daad-alumni.de

1. Introduction

Ironstones are non-cherty, sandy fine-grained siliciclastic or siliciclastic-carbonate sedimentary rocks with >15 wt.% iron, corresponding to 21.4 wt.% Fe_2O_3 (Petránek and Van Houten, 1997). The ironstones may or may not contain >50% ooids, pisoids, peloids and oncoids. Ooids are spherical or ellipsoidal coated-grains □2 mm in diameter, which display regular concentric laminae surrounding a central core. Grains similar to ooids, but >2 mm are known as pisoids. Oncoids and pisoids also differ in that the former have a biogenic origin and irregular concentric laminae (Flügel, 2010). Peloids are fine-grained material with diameters similar to ooids and pisoids, but without recognizable internal structure. These coated-grains, particularly ooids, were formed in either continental or marine depositional environments by biotic or abiotic pathways (Young and Taylor, 1989). The abiotic mechanisms for the formation of the coated-grains were reviewed by Van Houten (1992), Petránek and Van Houten (1997), and Collin et al. (2005). The microbial activity played a significant role in the formation of the ferruginous ooids, oncoids, and ferruginous stromatolite of the Lower Jurassic Minette oolitic ironstones, Lorraine, France (Dahanayake and Krumbein, 1986); the ferruginous oncoids, ooids, and ferruginous stromatolitic microbialites of the Aalenian and Bajocian of the Swiss Jura Mountains (Burkhalter, 1995); Middle Jurassic ferruginous ooids, Normandy, France (Préat et al., 2000); and the ferruginous oncoids, ooids, and ferruginous stromatolitic microbialites of northwestern Egypt (El Aref et al., 2006 b). Detailed investigations of the origin and mineralogy of oolitic

2

ironstones are restricted to a relatively small number of the worldwide Phanerozoic ooidal ironstone deposits (Young and Taylor, 1989; Mücke and Farshad, 2005).

The Middle Eocene ironstone deposits of El Bahariya Depression represent the only economic ooidal ironstone along the Tertiary paleo-Tethyan shorelines in northern Africa and southern Europe. These economic deposits represent the main exploitable iron ore deposits of Egypt since 1973 till now. They are located in the northeastern part of El Bahariya Depression, Western Desert, Egypt. The iron ore deposits are developed at the Ghorabi, El Harra, and El Gedida mines (Fig. 1). In contrast to the Middle Eocene ironstones of El Bahariya Depression, all other Cenozoic ooidal ironstone of the world are uneconomic to marginally economic and only few of these have been studied in detail (Van Houten, 1992; Petránek and Van Houten, 1997). The ooidal ironstones have a peak in abundance in the Early and Middle Eocene times that reflects major changes in the paleogeographic position of the shoreline during that time. Most of the Cenozoic ooidal ironstones, including El Bahariya ironstones, accumulated in shallow marine environments (Van Houten, 1992; Helba et al., 2001; El Aref et al., 2006 a). They were developed during relatively long periods of open circulation, low sedimentation rate, abundant burrowers, and normal amounts of marine fauna and micro-organisms. The ironstone deposits are commonly associated with phosphates and iron laterites. Although most deposits have no direct relation to volcanism (Van Houten, 1992), a few workers suggested a volcanic origin for the Phanerozoic ooidal ironstones (Heikoop et al., 1996; Sturesson et al., 1999, 2000; Sturesson, 2003). In northern Africa, Cenozoic ooidal ironstones occur in mixed siliciclastic-carbonate sequences associated with manganiferous and phosphatic mineralization (Petránek and Van Houten, 1997).

The present contribution aims at studying the mineralogical composition and geochemical characteristics of the different Middle Eocene marine ironstone facies of El Bahariya Depression, Western Desert, Egypt. It also sheds light on the syn- and post-Middle Eocene

subaerial weathering and subsurface alteration events that affected the original marine ironstones.

2. Geologic setting

El Bahariya Depression is a large, oval-shaped, NE-oriented depression in the center of the Western Desert (Fig. 1). Its maximum length is about 94 km, whereas its greatest width is about 42 km. It has a surface area of about 1800 km^2 and it is on all sides by a karst plateau of Cretaceous and Eocene carbonates. The plateau surface rises about 250 m above the present-day sea level. The floor and the basal part of the surrounding escarpment of El Bahariya Depression consist of Early Cenomanian clastic rocks of the Bahariya Formation. The study area includes the Gabal Ghorabi-Nasser (3.5 km^2), El Harra (2.9 km^2), and El Gedida (6.5 km^2) mine areas.

El Bahariya Depression is deformed by a NE-trending right-lateral wrench fault system (Fig. 1), which is associated with several doubly plunging folds and extensional faults (Sehim, 1993; Moustafa et al., 2003). Mapping of El Bahariya Depression also revealed the presence of three ENE-trending fault zones (Fig. 1). The maximum deformation is recorded in the two northern fault zones; Gabal Ghorabi-El Ghaziya and El Gedida-El Harra. The areas surrounding the master faults show small-scale doubly plunging anticlines represented by Early Cenomanian swells in the northeastern plateau of El Bahariya Depression. These swells include the three mine areas, which are almost aligned in an en-echelon pattern along the main NE-striking wrench faults.

In the three mine areas, the Middle Eocene ironstone succession forms an unconformity-bounded condensed section and shows a facies change towards the equivalent carbonate rocks of the surrounding plateau (El Aref et al., 1999, 2006 a; Helba et al., 2001). The Middle Eocene ironstones overlie the Early Cenomanian glauconitic sandstones and mudstones of the Bahariya Formation. The Bahariya Formation hosts uneconomic stratiform ironstone and iron sulfide bands and lenses.

The ironstone succession is composed mainly of autochthonous/para-autochthonous facies,

4

which are rich in ferruginous ooids, peloids, oncoids, and various ferruginized skeletal particles (Helba et al., 2001; El Aref et al., 2006 a). These facies are stacked in two shallowing-upward sequences (Fig. 2A). The lower ironstone sequence shows a lateral facies change due to paleotopographic variations of the underlying Bahariya Formation. This sequence originated as a lagoonal manganiferous mud-ironstone facies in the Gabal Ghorabi and El Harra mine areas (Fig. 2B). This facies changed laterally, in the central sector of Gabal Ghorabi and El Gedida mine areas, to an intertidal stromatolitic ironstone facies. The lagoonal setting was developed in paleolows created between the syn- and post-Cenomanian folds of the underlying Bahariya Formation. The tidal flat setting was dominant on the flanks of Gabal Ghorabi, El Harra and El Gedida paleo-highs. The manganiferous mud-ironstone facies is overlain by a storm-related fossiliferous ironstone facies and shallow subtidal-intertidal nummulitic-ooidal-oncoidal ironstone facies in the northern and southern sectors of Gabal Ghorabi mine area (Fig. 2A). The stromatolitic ironstone facies is overlain by the nummulitic-ooidal-oncoidal ironstone facies (Fig. 2C). The stromatolitic ironstone facies consists of even to slightly wavy laminae at its base that grades upward into micro-columnar and micro-domal stromatolitic types. The nummulitic-ooidal-oncoidal ironstone facies consists of five shallowing upward cycles. Each cycle begins with matrix-supported mud-/wacke-ironstones grading upward into grain-supported ooidal, oncoidal, and nummulitic pack-/grain-ironstones. These cycles reflect deposition under quiet water conditions that were interrupted by episodic storm waves. The quiet water conditions can be inferred from the presence of gradual contacts between the cortical laminae and the surrounding matrix, which are of the same composition. The textural and internal microfabric evidence reveals neither tangential, nor radial internal structures, but rather a random microfabric. Agitation during the wave episodes periods can be inferred from the presence of cross and graded bedding, and associated scour and fill structures. Moreover, some oncoids exhibit multi-phase encrustations, representing abrasional events and reworking during their development. The main components of the nummulitic-ooidal-oncoidal ironstone facies are

5

ferruginous ooids, peloids, oncoids, and skeletal particles. The skeletal particles include large benthic foraminifera (e.g. nummulitids and alveolinids), echinoderms, pelecypods and gastropods. During the calm periods, microbial communities represented by iron-oxidizing bacteria, flourished and developed at the water-sediment interface, and formed microbially mediated ooids, oncoids, and cortoids. The cortoids consist of microbored ferruginized bioclasts enveloped by a thin and unlaminated rind of amorphous iron oxyhydroxides. The cortoids represent an early stage of ooid and oncoid formation.

The upper ironstone sequence formation began by the deposition of shallow subtidal green mudstone facies, which represents a new marine transgression (Fig. 2D). The mudstone facies mainly composed of kaolinite, quartz, glauconite, halite, and relics of authigenic barite. This facies grades upward into intercalated bioturbated mud-ironstone and nummulitic-bioclastic ironstone facies.

The upper surfaces of the two marine ironstone sequences were subjected to subaerial weathering and pedogenesis. Infiltrating surface water formed a network of solution channels and small- to large-scale caves and vugs. The main recorded pedogenic features include desiccation cracks, alveolar texture (root mouldic porosity), ironstone breccias, goethite stalactites and stalagmites, cockade structures (rhythmic crustified colloform goethite and hematite layers surrounding breccias fragments), and cavity and cave fillings of goethite with botryoidal fabrics. The subaerial weathering was more intense in the upper ironstone sequence relative to the lower ironstone sequence.

3. Analytical methods

Samples from the different marine ironstone facies and lateritic iron ores were collected from the three mine areas and investigated by a variety of mineralogical, chemical, and spectroscopic techniques. The micro- and nano-morphological characteristics of the iron and manganese minerals and the microbial forms were preliminary investigated using a Jeol JSM-7001 field emission scanning electron microscope attached to an Energy-dispersive X-ray spectroscopy

6

(EDAX) unit. Subsequent SEM-EDAX analyses were carried out in the Otto-Schott-Institute of Glass Chemistry, Friedrich-Schiller University, Jena, Germany.

3.1. Whole-rock analytical techniques

The bulk mineralogical composition of the different marine ironstone facies and lateritic iron ores were performed on powdered samples by using a Seifert-FPM XRD7 powder diffractometer with Rayflex-Software. The device contains a Cu $K\alpha$ radiation source filtered with a nickel foil and Soller slits placed in the diffracted beam. The XRD analyses were done using 40 KV and 30 mA. Chemical analyses were performed on whole rock powders by X-ray Fluorescence (Philips PW 2400). The major elements were determined on fused beads (glass discs), in which the sample material was diluted with a flux agent in a ratio of 1:10 in order to minimize matrix effects. The whole rock trace and rare earth elements were measured by ICP-MS/OES. The powder samples were dissolved by HF and $HClO_4$ and subsequently analyzed by the Quadropole ICP-MS Series II (ThermoFisher Scientific, Bremen, Germany). All data were calculated to the dry mass and are given in $\mu g/g$ (Tables 1and 2). The XRD and XRF analyses were carried out in the Institute of Earth Sciences, Friedrich-Schiller University, Jena, Germany.

3.2. Micro-analytical techniques

Samples from the different ironstone facies were broken into small pieces with fresh surfaces for Raman spectroscopic analyses. This method was used to identify the mineralogical composition and types of organic matter and microcrystalline minerals. Raman spectra were recorded with a micro-Raman setup (HR Lab Ram inverse system, Jobin Yvon, Horiba). The Raman spectroscopic analyses were carried out in the Institute of Physical Chemistry, Friedrich-Schiller University, Jena, Germany (Ciobota et al., 2011).

The mineral chemistry of the different iron and manganese minerals was determined by Electron Probe Microanalyses (EPMA) and the element distribution maps within the ferruginous ooids were carried out by EDAX. The EPMA were performed on a JEOL JXA 8900 RL device at the Center of Geosciences, Department of Geochemistry, Georg-August University, Göttingen,

7

Germany. Analyses were made on carbon-coated polished-thin sections, injected with blue-dyed epoxy, to indicate the presence of porosity. The analyses were made at beam conditions of 15 kV and 15nA beam current. The micro-chemical analyses of the trace elements were done by Laser ablation ICP-MS through many profiles along ferruginous oncoids and surrounding cement and matrix. Laser ablation analyses were done by quadropole ICP-MS with a VG Microprobe II laser system (using Nd: YAG, 266 nm UV laser beam with a flat profile and 4mJ laser energy on the sample surface). The laser ablation system can define target locations for analysis and adjusts crater sizes from 5 μm to 400 μm. The laser ablation ICP-MS analyses were carried out in the Institute of Earth Sciences, Friedrich-Schiller University, Jena, Germany.

The X-ray photoelectron Spectroscopy (XPS) is a highly surface-sensitive technique that is used in many different areas of chemistry. This technique provides information about the oxidation and structural states, and determines the adsorped chemical species, on the surface of the iron oxides. The XPS analyses were carried out by Physical Electronics /Quantum 2000 XPS device. They include general survey scans (area =100 x 100 μm^2) and high resolution analyses of the iron peaks. The measurement time during the survey scans was 30 minutes and the pass energy was 117.4 eV. The high resolution XPS analyses of the Fe2p3 peaks were measured with pass energy at 58.70 eV and the measurement time was 60 minutes. All spectra were calibrated using C 1s peak with a fixed value of 284.8 eV. The XPS analyses were carried out in the Institute of Material Science and Technology, Friedrich-Schiller University Jena, Germany.

4. Results

4.1. Mineralogy

According to the field and microscopic observations, as well as facies analyses, the studied ironstone facies are subdivided into three main types.

The first type includes manganiferous mud and fossiliferous ironstone, which may be brick red, violet, or black. Microscopically, the mud-ironstone facies consists mainly of hematite spindles surrounded by goethite rims (Fig. 3A). Detrital minerals, such as quartz, rutile, and feldspars

(orthoclase and microcline), were derived from the underlying glauconitic sandstones of the Bahariya Formation. Authigenic clay minerals, such as kaolinite and illite, are diagenetically developed at the expense of feldspars (Fig. 3B, 3C). Secondary pore-filling manganese minerals, such as todorokite, birnessite, aurorite, manjiroite, romanèchite, hollandite, and pyrolusite, are developed between the hematite spindles. Todorokite is the dominant manganese mineral and it has a platy morphology in SEM and a plumose-like shape in the BSE images (Fig. 3B, 3D). Most of these minerals, particularly the manganese minerals, are only identifiable by micro-Raman Spectroscopy (spot analyses) and it is difficult to make a quantitative statement about their occurrences (Fig. 4). The clay minerals are only identified by SEM/EDAX, whereas XRD was only capable of identifying hematite, goethite, quartz, and kaolinite (Fig. 5).

The second ironstone type includes the microbially mediated stromatolitic and nummulitic ooidal-oncoidal facies. The ferruginous stromatolites, ooids, and oncoids components consist of yellowish-brown nanocrystalline iron oxyhydroxides and/or microcrystalline goethite laminae (Fig. 6A-6D). The iron oxyhydroxide laminae alternate with microbial laminae that are rich in heavily mineralized iron-oxidizing bacteria (Fig. 6E, 6F). The microbial morphologies of the iron-oxidizing bacteria were identified by SEM. Organic components, such as proteinaceous compounds, lipids, celluloses, and carotenoids were only identified by Raman spectroscopy (Fig. 7). These may represent remains of bacteria, fungi, and algae. Goethite is the essential mineral in the microbially mediated ironstone facies (Fig. 5). Under SEM, the nanocrystalline goethite phases (50 to 100 nm) have spherical and rod-like morphologies (Fig. 6C). Authigenic apatite crystals were identified by SEM-EDAX, BSE images, and Raman spectroscopy (Fig. 8). The morphology of apatite was confirmed by SEM as single short hexagonal prisms or twinned crystals restricted to certain ooid and oncoid cortical laminae (Fig. 8A). Psilomelane, jarosite, and quartz are the essential secondary mineral association in the microbially mediated ironstone facies. Secondary psilomelane is associated with the green $FeSO_4$ laminae as concordant

discontinuous laminae or as secondary fracture filling phases (Fig. 9A, 9B). Under SEM, the psilomelane exhibits either isolated fibrous nests or a platy habit (Fig. 9C, 9D).

The third ironstone facies type includes the lateritic iron ores that were formed by alteration at the upper surface of both ironstone sequences. Microscopically, goethite and hematite, with colloform, botryoidal, cavernous, tabular, and globular textures, are developed in the solution features (Fig. 10A-10C). Mineralogically, goethite and hematite are the main iron minerals in the lateritic iron ore (Fig. 5). Authigenic clay minerals, such as illite, detrital quartz, and feldspars, cavity filling psilomelane, calcite, nitratine, gypsum, anhydrite, halite, rapidcreekite, and barite are detected by Raman spectroscopy.

4.2. Geochemistry

4.2.1. Whole-rock geochemistry

The geochemical characteristics of the marine ironstones and lateritic iron ores depend mainly on the mineralogical compositions. Two phases appear to control the bulk major and trace elements compositions: iron oxides and iron and manganese oxyhydroxides. The enrichment factor of the major and trace elements is calculated by comparing the mean chemical compositions of the different iron ore types and the composition of the upper continental crust for all major and trace elements (Taylor and McLennan, 1985), except for S and Cl (Wedepohl, 1995).

The manganiferous mud and fossiliferous ironstone facies consists mainly of hematite and manganese minerals together with authigenic clay minerals and detrital components including heavy minerals. These mineralogical compositions were reflected in the major oxide analyses of the facies.

In the manganiferous mud-ironstones (Gh2 and Hr5), Σ (Fe$_2$O$_3$+MnO$_2$) = ~ 93 wt.%, Σ (K$_2$O+ Na$_2$O+ CaO+ MgO) ranges from 1.75 wt.% to 1.55 wt.%, and Σ (SiO$_2$+ Al$_2$O$_3$) = ~ 3 wt.% (Table 1). In the mud-ironstone paleosols of the lower ironstone sequence (Gh3 and Gh14), Σ (Fe$_2$O$_3$+MnO$_2$) ranges from 78 wt.% to 86 wt.%, Σ (K$_2$O+ Na$_2$O+ CaO+ MgO) ranges from 3.42

10

wt.% to 3.88 wt.% and Σ (SiO_2+ Al_2O_3) ranges from 8 wt.% to 17 wt.% (Table 1). The TiO_2 is higher in the paleosols than in the manganiferous mud-ironstones. The relative increase in SiO_2 and Al_2O_3 in the paleosols indicates the presence of kaolinite, illite, and detrital quartz as confirmed by SEM. The slight increase in K_2O, Na_2O, and CaO is inferred from the presence of detrital feldspars, whereas the slight increase in MgO is mainly related to the presence of todorokite. The presence of rutile as a detrital heavy mineral reflects the slight increase in TiO_2 in the paleosols.

The enrichment factor of the manganiferous mud and fossiliferous ironstone facies indicates that they are highly enriched in Ba, Cl, Mo, Pb, S, U, and Zn, and slightly enriched in Eu, Sr, and V (Fig. 11A).

The microbially mediated ironstone facies consists mainly of FeOOH and SiO_2. In this facies, goethite is the main mineral, whereas quartz mainly occurs as a cement of the ferruginous ooids, oncoids, and rarely occurs as a detrital component. Low concentrations of Al_2O_3, which ranges from 1.02 wt.% to 2.28 wt.%, are related to the small amount of authigenic clay minerals. Samples Gd3, Gh5, and Gh8 contain relatively higher MnO_2 than other samples due to the presence of manganese minerals as cementing materials and/or fracture-filling pyrolusite and psilomelane. The relative increase in CaO, Na_2O, and SO_3 in sample Gh9 is attributed to the presence of late cementing minerals, such as gypsum, calcite, and halite (Table 1).

The enrichment factors of the microbially mediated ironstone facies indicate that it is highly enriched in Zn, V, Mo, U, S, and Cl and slightly enriched in P, Cr, and Ni (Fig. 11B). Because the ferruginous ooids and oncoids are cemented by hematite and psilomelane cement, the nummulitic-ooidal-oncoidal ironstone facies is enriched in manganophile elements such Ba and Co (Fig. 11C).

The lateritic iron ore of El Gedida mine area (samples Gd6, Gd.8, Gd11, Gd16, and Gd17) consists mainly of $\Box$ 90 wt. % Fe_2O_3, whereas the lateritic iron ore of Ghorabi mine area (samples Gh16, Gh17, and Gh20) consists of $\Box$ 80 wt. % Fe_2O_3 (Table 2). The decrease in Fe_2O_3

11

is related to the increase in MnO_2, SiO_2, Na_2O, and CaO. The relative increase in MnO_2, SiO_2, Na_2O, and CaO is due to the presence of detrital quartz and late cavity- and fracture-filling mineral phases such as halite, calcite, gypsum, anhydrite, and psilomelane. The lateritic paleosol covering the lower ironstone sequence in El Harra mine area (samples Hr6, Hr8, and Hr11) consists mainly of Fe_2O_3, which ranges from 75 wt.% to 85 wt.% (Table 2). The decrease in Fe_2O_3 is attributed to the increase in SiO_2 and P_2O_5. The slight increase in Al_2O_3 and SiO_2 is probably due to the presence of illite. The pronounced increase in SiO_2 in sample Hr11 is due to the presence of detrital quartz. The increase in P_2O_5 is also linked to clay minerals as indicated by the EDAX analyses. The increase of Na_2O is related to halite as indicated by XRD.

The enrichment factors of the lateritic iron ore type indicate that it is highly enriched in Zn, Mo, Ba, Pb, and Cl, and slightly enriched in P and U (Fig. 11D). The paleosol capping the lower ironstone sequence of El Harra mine is highly enriched in P, Zn, V, Mo, Pb, U, S, and Cl and slightly enriched in Ti, La, Cr, Ba, and Ce (Fig. 11E).

All the marine ironstone facies and the lateritic iron ore and paleosols are enriched in Zn, Mo, U, S and Cl. They are also depleted in alkali and alkaline earth elements, such as Mg, Na, and K, because they are highly mobile elements and thus easily leached during surface and subsurface alteration processes

In addition to the bulk analyses of the trace elements, many detailed profiles within the ferruginous oncoids and stromatolite columns were measured by using laser ablation ICP-MS. This allowed study of the micro-chemical variations of major, minor, and trace elements, and definition of the correlation of the trace elements with iron and manganese oxides and oxyhydroxides. There is a positive correlation between Fe and Al, K, P, V, Cr, Zn, Mo, As, and Ni on one hand, and positive correlation between Mn and the manganophile elements, such as Co, Ba, and Pb on the other (Figs. 12, 13). Silica increased with the silica cement, whereas Ti is in very low and constant concentrations in the ooids and oncoids cortices and cements.

The REE concentrations measured by ICP-MS are normalized to chondrite, and Ce and Eu

anomalies are calculated based on $\Delta Ce=2xCe_{CN}/(La_{CN}+Pr_{CN})$, $\Delta Eu=2xEu_{CN}/(Sm_{CN}+Gd_{CN})$, LREE= Σ La$_{CN}$ to Eu$_{CN}$/6, HREE=Σ Gd$_{CN}$ to Lu$_{CN}$/8 and ΣREE= total sum of REE (Tables 1, 2). All values are chondrite-normalized (CN). The REE mobility is controlled mainly by the redox potential of the local environment; therefore, REE patterns can be used in tracing post-depositional diagenetic processes. Furthermore, conditions that are more oxic would lead to REE enrichment (Ingri, et al., 2000). Variations in cerium probably are controlled by redox reactions because Ce has two oxidation states: Ce^{3+}, similar to the majority of lanthanides, and Ce^{4+}. However, unless Ce^{4+} is strongly complexed in oxidizing conditions, it is almost never present in aqueous solutions (De Barr et al., 1985). Fractionation of cerium in seawater is dependent upon redox potential. Cerium is a well-known, redox-sensitive REE, and has a potential paleo-redox value in marine environments. Negative Ce values and LREE depletion result from depletion of Ce or fractionation by precipitation with iron and manganese oxides. Thus, negative Ce anomalies in the stromatolitic and ooidal-oncoidal ironstone facies indicate oxidizing marine conditions (Fig. 14A). During the subaerial weathering, the highly mobile HREEs can be removed during the dissolution processes (Fig. 14A). The loss and gain calculations of the ooidal-oncoidal ironstone facies and the superimposed subaerial weathering processes indicate that the lateritic iron ore is enriched in the LREEs and depleted in the HREEs relative to the ooidal-oncoidal ironstone facies (Fig. 14B). This may indicate loss of the HREEs during the subaerial weathering processes and their concentration in the ooidal-oncoidal ironstone facies.

4.2.2. Mineral Chemistry

The chemistry of goethite and hematite of the different ironstone facies was studied by EPMA and EDAX. The structural formula of goethite was calculated on the basis of 1 (O) and 1 (OH) and hematite was calculated on the basis of 3 (O). The goethite of the ooidal-oncoidal and stromatolitic ironstones is generally Al-poor, where the Al$_2$O$_3$ rarely exceeds 2% (Table 3). Element maps were made in the ferruginous ooid and oncoid cortices for Fe, Si, Al, Mn, K, Ba, Mg, and Ca (Fig. 15). The distribution of Al in the cortices of ferruginous ooids and oncoids

13

was a homogenous within iron oxyhydroxides or more local in clay minerals. The presence of Al in iron oxyhydroxides and clays is consistent with EDAX spot analyses and SEM analyses, respectively.

The distribution of Mn, Ba, and K in the cortices of ooids and oncoids is related to the discontinuous psilomelane laminae (Fig. 15). The precise chemical analyses were obtained by EPMA. Some psilomelane laminae still have transitional phases, where Fe and Mn exist together as indicated by the EPMA (Table 4). The distribution of Si in the cortices of ooids and oncoids is related to the cavity-filling microcrystalline quartz (Fig. 15). The element maps of the Ca and Mg showed that they are homogeneous in their distribution and their concentrations are limited. Calcium may be concentrated in small areas, which is probably related to the presence of apatite, calcite, gypsum, or anhydrite. Todorokite was also analyzed by EPMA and EDAX spot analysis, and this showed that it is the host mineral for zinc in the manganiferous mud-ironstone facies.

The colloform goethite and hematite in some samples (Gh18) have a slight excess in SiO_2. The EPMA and EDAX analyses of the green cortical laminae are very difficult to interpret and less reliable because of their highly porous nature that indicates corrosion and dissolution, as well as because of the presence of gypsum and anhydrite. This was the main reason in the application for the XPS to identify the ideal chemical composition of these laminae.

The XPS survey scans of the green-colored cortical laminae indicate the presence of Fe, O, C, Cl, S, Na N, Zn, Ti, Si, Ca and P (Fig. 16A). For studies involving iron oxides, the Fe $(2p_{3/2})$ peak and the O (1s) peak are the most commonly scanned peaks (Cornell and Schwertmann, 2003). The high resolution of the Fe $(2p_{3/2})$ peak indicates that ferrous iron is linked to the SO_4^{2-} ligand (Fig. 16B). The shift in the Fe $(2p_{3/2})$ peak binding energy (712.1 eV) corresponds to $FeSO_4$ as a main component of the green laminae. The shift in the O (1s) peak corresponds to oxygen, phosphate and Fe_2O_3 speciation; the shift in the Ca (2p) peak corresponds to $CaCO_3$, $CaSO_4$, and $Ca_5(PO_4)_3(F,Cl,OH)$; the shift in the N (1s) peak corresponds to NO_3; the shift in the Si (2s) peak may be inferred to correspond to amorphous silica (Kennedy et al., 2003); and the

shift in the P (2p) peak corresponds to phosphate.

In addition to the green FeSO₄ laminae, the XPS survey scans of the yellowish-brown cortical laminae of the ferruginous oncoid indicate the presence of Fe, O, C, N, Na, Cl, Ca, Si, and K. The high resolution of the Fe ($2p_{3/2}$) peak indicates that ferric iron is linked to an OH ligand. The shift in the Fe ($2p_{3/2}$) peak binding energy (711.2 eV) corresponds to a αFeOOH species. Moreover, the XPS survey scans of the surrounding cement between the ferruginous ooids and oncoids indicate the presence of Fe, O, C, Mn, Na, Cl, N, and Si. The high resolution of the Fe ($2p_{3/2}$) peak indicates that ferric iron is linked to O^{2-} ligands. The shift in the Fe ($2p_{3/2}$) peak binding energy (710.8 eV) corresponds to αFe_2O_3 species.

5. Discussion

The application of different mineralogical and geochemical techniques in studying El Bahariya ironstones, particularly the ferruginous ooids and oncoids, provided more precise information about the mineralogical composition, organic content, and diagenetic evolution than previous studies on the genesis of Cenozoic iron ores. The mineralogical composition and geochemical character of El Bahariya ironstones vary according to the different depositional and diagenetic processes, as well as to the superimposed surface and subsurface alteration processes.

5.1. Depositional and diagenetic processes

The depositional processes of ironstones formed in marine setting depend on many variables that include water depth, pH, Eh, organic matter, topography of the depositional basin, and fluxes of detrital and dissolved compounds to the marine depositional environment. The precursor materials consist of colloidal iron oxyhydroxides, as well as limited amounts of reworked siliciclastic rocks from the underlying Bahariya Formation. The oxyhydroxides might have been transported to the depositional basin as colloidal suspensions by a river system. They settled in quiet water, forming either burrow-mottled mud-ironstone facies in a lagoonal setting or stromatolitic ironstone facies in a tidal flat setting. On the other hand, the nummulitic-ooidal-oncoidal ironstone facies was deposited in intermittently quiet and agitated water condition (El

15

Aref et al., 2006 a). The benthic microbes contributed to the precipitation of the colloidal iron oxyhydroxides as a ferric gel surrounding their cell surfaces (Parenteau and Cady, 2010; Konhauser et al., 2011). The net result of this process is the formation of amorphous and nanocrystalline iron oxyhydroxides (El Aref et al., 2006 b).

There is common agreement that ooidal ironstones can form in both marine and continental sedimentary environments. However, in the present study, a continental origin, as suggested by Siehl and Thein (1989), can be excluded for the studied ooidal ironstones because benthic foraminifera and skeletal algae are associated together with or sometimes incorporated into the cortex of the ferruginous ooids and oncoids. Also, the near absence of any calcareous ooids and oncoids from the surrounding equivalent carbonate succession indicates that the ferruginous ooids and oncoids are plausibly primary depositional grains (Helba et al., 2001; El Aref et al., 2006 a). They are neither inherited calcareous coated-grains that were subsequently replaced by an iron-bearing hydrothermal solution (Basta and Amer, 1969), nor lateritic ooids and pisoids derived from hinterlands and reworked to the marine environment (Siehl and Thein, 1989). The lack of Al- for Fe-substitution in the goethite structure, as shown by our unpublished FTIR spectroscopy, can be considered as an additional argument against the continental origin. The internal nanostructures of the cortical laminae of both ferruginous ooids and oncoids revealed that they are primary depositional grains. The nanostructures of the cortical laminae consist of nanocrystalline spherical aggregates that diagenetically evolved into short ragged nanorods and then well crystallized euhedral goethite. These nanostructures, which are neither tangential, nor radial, may also reveal that these grains are autochthonous in origin. The common presence of apatite crystals inside the cortical laminae of both ooids and oncoids may strengthen the argument for a marine origin of these grains because apatite crystals are lacking in the continental oolites (Schwarz and Germann, 1993). They were later *in situ* reworked together with the ferruginized skeletal particles along the sea bottom by tidal and/or storm waves, forming cross-bedded and megarippled parautochthonous ironstone facies.

16

A submarine-hydrothermal deep-water iron source cannot be considered here because there is no Middle Eocene volcanism known in the region. On the other hand, hydrothermal activity associated with Oligocene-Miocene volcanic events could have overprinted the primary marine ironstone deposits.

The primary marine ferric iron oxyhydroxide colloid/gel and the microbial biomass underwent several diagenetic modifications. Goethite is a primary early diagenetic phase, which is formed after the dehydration and recrystallization of the precursor ferric-iron colloid/gel phase within an essentially oxic zone (Hughes, 1989; Raiswell, 2011). These processes are inhibited or retarded in the presence of organic compounds, and phosphate and silicate species (Cornell and Schwertmann, 2003). The EDAX analyses of the primary iron oxyhydroxides indicated the presence of Fe, P, Ca, and Si. The presence of such organic compounds and the phosphate and silicate species associated with the microbially mediated ironstone facies could have been significant in preventing diagenetic recrystallization and dehydration processes from forming additional hematite (Cornell and Schwertmann, 2003). On the other hand, the absence of such compounds in the fossiliferous and mud-ironstones could have promoted the dehydration of goethite to form hematite.

Most marine environments are oxic, and as a result, $\geq 90\%$ of the organic carbon of the marine sea floor sediments is oxidized close to the sediment-water interface. This process occurs through microbial breakdown of the organic matter and its transformation into simple molecules and inorganic species (Chester, 2003). The relict organic compounds were identified by Raman spectroscopy as proteinaceous compounds, lipids, carbohydrates, and carotenoids, which are enclosed in dense nanocrystalline iron oxyhydroxide aggregates. These organic materials may represent remains of bacteria, fungi and algae. The organic matter was mostly degraded during early diagenesis, when the microbes consumed the oxygen in the breakdown of the organic molecules. Small amounts of organic material were probably preserved within the iron oxyhydroxide structures (e.g., Ingalls et al., 2004). Inorganic compounds, such as phosphates,

sulfates, and silicates, are detected by different chemical and spectroscopic techniques. The formation of phosphate minerals such as calcium fluorapatite, is intimately associated with microbial activity. Phosphates are released into interstitial pore waters via microbial degradation of organic matter and adsorbed to the iron oxyhydroxide surfaces. Locally high rates of phosphate release can promote the rapid nucleation of amorphous calcium fluorapatite phases through sediment pore water and on the surfaces of iron oxyhydroxide (Tribovillard, et al., 2006; Konhauser, 2007). Diagenetic recrystallization led to the dehydration of goethite to form hematite, possibly during an arid climate (Gehring, 1989; Schwertmann, et al., 2004; Raiswell, 2011).

5.2. Potential surface weathering and subsurface alteration processes

Hydrogeological studies of El Bahariya Oasis indicated that local groundwater is a mixture of deep artesian groundwater inflow and surface pluvial recharge (Dabous, 1994, 2002). Each water type has had its own impact on the mineralogy and geochemistry of the original marine ironstone sequence. The marine ironstone sequences were subjected to syn- and post-Middle Eocene tectonic uplift that led to their exposure to subaerial weathering processes and pedogenesis.

Subaerial weathering took place under warm and humid, then subsequent arid climatic conditions. Under the warm and humid climate, the supergene enrichment of iron occurred via the infiltration of surface meteoric fluids through the syn- and post-Middle Eocene fracture systems. Repeated mineral dissolution and reprecipitation along fractures and within cavities included formation of: 1) goethite and hematite stalactites and stalagmites with botryoidal and colloform textures, 2) cockade textures where ooidal ironstone breccias are cemented by crustified layers of colloform goethite, 3) small-scale alveolar voids at sites of former plant roots, and 4) vadose meniscus cement and desiccation cracks. The subaerial weathering also partly obliterated the sedimentary structures, fabrics, and textures of the original marine ironstones. Recent weathering events under more arid conditions, perhaps within the past 10000

18

years, have been recorded by U-Th isotope applications (Dabous, 2002). Newly formed goethite and hematite are the main lateritic iron ore minerals and have a relative excess of Al with respect to Fe in comparison with the original Eocene marine ooidal ironstones. The Al content of goethite ooids is an important key factor in understanding the genesis of the ironstones (Fitzpatrick and Schwertmann, 1982; Maynard, 1986). Detrital quartz and feldspars are probably concentrated with the lateritic iron ore by wind action. Authigenic illite and kaolinite were formed in situ at the expense of detrital feldspars. Cavity-filling mineral phases, such as psilomelane, calcite, nitratine, gypsum, anhydrite, halite, rapidcreekite, and barite, are formed as a result of more recent precipitation during arid climatic conditions.

In addition to subaerial weathering, the marine ironstones have also been altered by circulating heated groundwaters. The microscopic investigations and the BSE images show evidence of dissolution, corrosion and fragmentation of the original yellowish-brown iron oxyhydroxide cortical laminae of the ferruginous ooids and oncoids. The corrosive green ferrous sulfate, black manganese patches and quartz are the main products of the alteration. The probable source of the ferrous sulfate compound is the oxidation of sulfides, primarily pyrite, by the groundwater. These sulfides are hosted in the glauconitic clays and black shales of the underlying Early Cenomanian Bahariya Formation (Abdel-Monem et al., 2003). The oxidation of pyrite generates solutions that are quite acidic (pH~$\leq$2) (Waychunas, et al., 2005; Taylor and Macquaker, 2011) and that contain high concentrations of SO_4^{-2}, Fe^{2+}, and H^+. El Bahariya well waters are uncommonly high in dissolved Fe and Mn, and had temperatures as high as 55 °C (El Shazly et al., 1991). In addition, Korany (1995) studied the deeper aquifer in El Bahariya mine area and reported high concentrations of 10.3 ppm Fe^{2+} and 27.5 ppm H_2S. The final alteration products are precipitated hydrous ferric sulfates, such as jarosite, and/or ferric oxyhydroxide and oxides, such as goethite and hematite (Gilbert and Park, 1986). Jarosite is typically thought to be a secondary mineral formed under arid weathering conditions by drying up the infiltrated $FeSO_4$ solution. It is generally agreed that jarosite is stable under highly acidic (pH < 3) and oxidizing

conditions (Singh *et al.*, 1999; Elwood Madden *et al.,* 2000). The oxidation processes can be catalyzed by microbial activity (Edwards et al., 2000), but no information exists for such in our study. The oxidation of pyrite can also promote the release of Mn^{2+} in the acidic conditions (Shippers and Jorgensen, 2001). In addition to SO_4^{2-}, Fe^{2+}, and Mn^{2+}, the oxidation of iron sulfides can also introduce high concentrations of redox-sensitive heavy metals into groundwater (Bowel and Bruce, 1995). Heavy metals, such as P, V, Zn, Ba, Ni, Mo, and U are most probably concentrated during the redox cycling of iron and manganese associated with the oxidation of pyrite. These elements, particularly P and V, could be released from the original marine microbially mediated ironstone facies and transported in the form of metal-organic complexes or adsorbed on the iron oxyhydroxides.

The laser ablation ICP-MS analyses indicated the manganophile elements, such as Zn, Ba, and Co, are associated with manganese oxides and oxyhydroxides. The manganiferous mud and fossiliferous ironstones are highly enriched in Zn, Mo, Ba, Pb, U, S, and Cl (Fig. 11A). Zinc is mainly concentrated within todorokite as indicated by EDAX analyses. Zinc is closely associated with the green ferrous sulfate laminae within the ferruginous ooids and oncoids as proved by XPS analyses. The presence of Zn in the green ferrous sulfate laminae suggest that during oxidation of iron sulfides, Zn was mobilized together with Fe^{2+} and SO_4^{2-}. Zinc is also enriched in the clay minerals, such as illite in the lateritic iron ore, as indicated by the EDAX analyses.

Barium and strontium are highly enriched in the manganiferous and fossiliferous ironstones and the lateritic iron ore, particularly in Ghorabi mine area. Barium is an essential element in psilomelane (hollandite and romanèchite) and todorokite. Barite is found in many stratigraphic levels of the ironstone sequences in the form of stratabound to stratiform barite cement, and also as rosettes at the contact between the underlying Bahariya Formation and the Middle Eocene ironstones. Stratiform barite nodules are hosted in the organic-rich green mudstone facies at the base of the upper ironstone sequence of Gabal Ghorabi mine area (EL Aref et al., 2006a). The

major barite deposits are the stratabound karst-related barite deposits in Ghorabi and El Gedida mine areas. They form cavity and fracture filling barite pockets and masses. The stratabound karst-related barite deposits were formed by secondary enrichment during dissolution and reprecipitation within solution cavities and fractures.

Under thes very acidic weathering conditions, Si is moderately soluble, Al is more soluble, and organo-metal complexes can be formed. This can further promote the breakdown of aluminosilicates to release Al as a soluble organic complex and precipitate quartz (Trescases, 1992).

In the arid environment, the strong evaporative concentration of dissolved components in surface and groundwater led to precipitation of a variety of cavity- and fracture-filling minerals. These included gypsum, anhydrite, halite, rapidcreekite, nitratine, jarosite and barite, calcite, manganese minerals (todorokite, psilomelane, pyrolusite) and quartz.

The XRF analyses indicated the presence of high amounts of S and Cl in all ironstone facies and the XPS analyses detected the presence of Na, Cl, N, and Si in the cortices and cement of both ferruginous ooids and oncoids. This may indicate recent depositional events after the Pleistocene pluvial periods, which caused mineralogical and chemical alterations typical of the young weathering crusts in the northeastern African Desert.

6. Conclusions

Based on the field, microscopic, mineralogical and geochemical investigations, the marine ironstone facies are subdivided into three types. The first type includes manganiferous mud and fossiliferous ironstone facies and the second type includes the microbially mediated ironstone facies that include stromatolitic and nummulitic-ooidal-oncoidal ironstones. The third type includes the lateritic iron ores, which demarcate the top surfaces of the lower and upper ironstone sequences as a result of the subaerial weathering processes.

Comprehensive mineralogical investigations indicate that the manganiferous mud and fossiliferous ironstone facies association consists mainly of hematite, whereas the microbially

mediated ironstone facies association consists mainly of goethite. The amorphous iron oxyhydroxides are the main precursor materials of these two minerals. The amorphous iron oxyhydroxides are recrystallized to goethite and then dehydrated to hematite. The recrystallization process of amorphous iron oxyhydroxides into goethite and/or hematite can be inhibited or retarded by the presence of organic and/or inorganic components. The microbial micromorphology still preserved in the cortices of the ironstone ooids is good evidence for their aquatic origin. Marine microorganisms associated with the ooids verify the marine origin of the ooidal goethitic ironstones.

The scarcity of Al in the goethite and hematite structures argues against the supergene origin of the ferruginous ooids and oncoids and confirms the primary marine origin.

Authigenic apatite and remains of organic materials are detected inside the stromatolitic and cortical laminae of the ferruginous ooids and oncoids, which indicates the role of biogenic processes in the formation of this facies association. Relict dolomite rhombs were detected in the nummulite structures, which may indicate that these fossil particles are dolomitized before the diagenetic ferruginization and replacement. Detrital minerals such as quartz, rutile, and feldspars, are observed in the mud and fossiliferous ironstones, as well as in the lateritic iron ores. These minerals are probably derived from the underlying Bahariya Formation. Authigenic clay minerals, such as kaolinite and illite, are abundant in the manganiferous ironstones and lateritic iron ores. They were formed at the expense of detrital feldspars.

The green ferrous sulfates, jarosite, manganese minerals, and quartz (as cement) are the main secondary minerals in the microbially mediated ironstone facies, and they are related to the subsurface alteration of rocks of the Bahariya Formation. Pyrolusite, hollandite, and romanèchite are the main manganese minerals in all iron ores. Other manganese minerals, such as todorokite, birnessite, manjiroite, and aurorite, were only observed in the mud and fossiliferous ironstone facies. The late cement minerals, such as barite, gypsum, anhydrite, rapidcreekite, nitratine, halite, and calcite, are observed in the all iron ores.

22

Geochemical analyses indicate that all ironstone types are enriched in the highly mobile elements, such as Zn, Mo, U, S, and Cl, and depleted in alkali and alkaline earth elements, such as Mg, Na, and K, compared to crustal average. Laser ablation ICP-MS profile analyses of the ferruginous ooids and oncoids indicate that there is a positive correlation between Fe and Al, K, P, V, Cr, Zn, Mo, As and Ni, and between Mn and the manganophile elements, such as Co, Ba, and Pb. Quartz is present as Si cement, whereas Ti is consistently in low concentrations in both cortex and cement. The geochemical behavior of the redox-sensitive minor and trace elements, such as V, Cr, Mn, Co, Ni, As, Mo, and U, depends mainly on the recycling of iron and manganese. Consequently, the redox gradient created during the acidification of the groundwater by the oxidation of pyrite, and formation of ferrous iron sulfates and jarosite, played a major role in the recycling and enrichments of these elements. The relative abundance of the biophilic elements, such as V, P, and Mo, in the ferruginous ooids and oncoids could be attributed to the microbial activity during their formation, whereas Ni and Zn behave as micronutrients in an oxic environment. Zinc is associated with todorokite in the manganiferous mud-ironstone facies, green ferrous sulfates laminae and the authigenic clays of the lateritic iron ores. Zinc is highly mobile element under weathering condition.

Acknowledgements

References

Abdel-Monem, A. A., Korany, E. A., Youssef, A. M., 2003. Occurrence and genesis of pyrite in El Gedida iron mine, El-Bahariya Depression, Western Desert, Egypt. Sedimentary Society of Egypt 11, 227-238.

Basta, E. Z., Amer, H. I., 1969. El Gedida iron ores and their origin, Bahariya oasis, Western Desert, U. A. R. Economic Geology 64, 424-444.

Bowel, R. J., Bruce, I., 1995. Geochemistry of iron ochres and mine waters from Levant Mine, Cornwall. Applied Geochemistry 10, 237-250.

Burkhalter, R. M., 1995. Ooidal ironstones and ferruginous microbialites: origin and relation to sequence stratigraphy (Aalenian and Bajocian, Swiss Jura mountains). Sedimentology 42, 57-74.

Chester, R., 2003. Marine geochemistry, 2nd ed. Blackwell Science Ltd, 506 p.

Ciobota, V., Salama, W., Tarcea, N., Rösch, P., El Aref, M., Gaupp, R., Popp, J., 2011. Identification of minerals and organic materials in Middle Eocene ironstones from the Bahariya Depression in the Western Desert of Egypt by means of micro-Raman spectroscopy. Journal of Raman Spectroscopy, DOI 10.1002/jrs.3047.

Collin, P.Y., Loreau, J.P., Courville, P., 2005. Depositional environments and iron ooid formation in condensed sections (Callovian–Oxfordian, south-eastern Paris Basin, France). Sedimentology 52, 969-985.

Cornell, R.M., Schwertmann, U., 2003. The iron oxides: structure, properties, reactions, Occurrence and Uses. VCH, Weinheim, Germany, 664 p.

Dabous, A. A., 1994. The geochemistry of uranium and thorium isotopes in the Western Desert of Egypt. Geochimica et Cosmochimica Acta 58, 4591-4600.

Dabous, A. A., 2002. Uranium isotopic evidence for the origin of the Bahariya iron deposits, Egypt. Ore Geology Reviews 19, 165-186.

Dahanayake, K., Krumbein, W. E., 1986. Microbial structures in ooidal iron formations. Minerlium Deposita 21, 85-94.

De Baar, H. J. W., Bacon, M. P., Brewer, P. G., Bruland, K. W., 1985. Rare earth elements in the Pacific and Atlantic Oceans. Geochimica et Cosmochimica Acta, 49, 1943- 1959.

Edwards, K. J., Bond, P. L., Druschel, G. K., McGuire, M.M., Hamers, R.J. Banfield, J. F., 2000. Geochemical and biological aspects of sulfide mineral dissolution: lessons from Iron Mountain, California. Chemical Geology 169, 383-397.

El Aref, M. M., El Sharkawi, M. A., Khalil, M. A., 1999. Geology and genesis of the stratabound and Stratiform Cretaceous-Eocene iron ore deposits of the Bahariya region, Western Desert, Egypt. GAW 4th Int. Conf., Cairo Univ., Egypt, 450-475.

EL Aref, M. M., Mesaed, A. A., Khalil, M. A., Salama, W. S., 2006 a. Stratigraphic setting, facies analyses and depositional environments of the Eocene ironstones of Gabal Ghorabi mine area, El Bahariya Depression, Western Desert, Egypt. Egyptian Journal of Geology 50, 29-57.

EL Aref, M. M., Mesaed, A. A., Khalil, M. A., Salama, W. S., 2006 b. Microbialite morpho-structures and biogenic accretion mechanism of the Eocene ironstones of Gabal Ghorabi mine area, El Bahariya Depression, Western Desert, Egypt. Egyptian Journal of Geology 50, 59-81.

El Shazly, M.M.; El Ramly, I.M.; Guindy, Kh.A. AND Abdel Aati, A., 1991. Bahariya formation water quality characteristics and its relationship to the hydrothermal activity in Bahariya Oasis, Western Desert, Egypt. Geol. Soc. Egypt. 29th Annual Meeting, Cairo, Egypt (Abstract).

Fitzpatrick, R. W., Schwertmann, U., 1982. Al Substituted goethite- an indicator of pedogenic and other weathering environments in South Africa. Geoderma, 7, 335-347.

Flügel, E., 2010. Microfacies of Carbonate Rocks. Analysis, Interpretation and Application. Springer-Verlag Berlin Heidelberg, Germany.

Gehring, A. U., 1989. The formation of goethitic ooids in condensed deposits in northern Switzerland, Geol. In: Young, T. P., Taylor, W. E. G., (Eds.), Phanerozoic Ironstones. Geological Society Special Publications London 46, 133-140.

Gilbert, J. M., Park, C. F., 1986. The geology of ore deposits. W. H. Freeman and Co., USA, 985 p.

Heikoop, J.M., Tsujita, C.J., Risk, M.J., Tomascik, T., Mah, A.J., 1996. Modern iron ooids from a shallow-marine volcanic setting: Mahengetang, Indonesia. Geology, 24, 759-62.

Helba, A. A., El Aref, M. M., Saad, F., 2001. Lutetian oncoidal and ooidal ironstone sequence; depositional setting and origin; northeast El Bahariya Depression, Western Desert, Egypt. Egyptian Journal of Geology 45/1A, 325-351.

Hermina, M., Klitsch, E., Lift, F., 1989. Stratigraphic lexicon and explanatory notes to the geological map of Egypt, 1:500000. Conoco Inc., Cairo, Egypt, 263p.

Hughes, C. R., 1989. The application of analytical transmission electron microscopy to the study of oolitic ironstones: a preliminary study. In: Young, T. P., Taylor, W. E. G., (Eds.), Phanerozoic Ironstones. Geological Society Special Publications London 46, 121- 131.

Ingalls, A. E., Aller, R. C., Lee, C., Wakeham, S. G., 2004. Organic matter diagenesis in shallow water carbonate sediments. Geochimica et Cosmochimica Acta 68, Number 21, 4363-4379.

Ingri, J., Widerlund, A., Land, M., Gustafsson, O., Andersson, P., Ohlander, B., 2000. Temporal variations in the fractionation of the rare earth elements in a boreal river; the role of colloidal particles. Chemical Geology, 166, 23-45.

Kennedy, C.B., Scott, S.D., Ferris, F.G., 2003. Ultrastructure and potential sub-sea floor evidence of bacteriogenic iron oxides from Axial Volcano, Juan de Fuca Ridge, north-east Pacific Ocean. FEMS Microbiology Ecology 43, 247-254.

Konhauser, K.O., 2007. Introduction to geomicrobiology. Blackwell Publishing Ltd, UK, 425 p.

Konhauser, K. O., Kappler, A., Roden, E. E., 2011. Iron in microbial metabolisms. Elements, 7, 89-93.

Korany, E. A., 1995. Hydrogeologic evaluation of the deeper aquifer in Bahariya mines area, Egypt. Symp. Nubian Sandstone rocks, Bengazy, Libya, Gume, 1-38.

Maynard, J. B., 1986. Geochemistry of ooidal iron ores, an electron microprobe study. Economic Geology, 81, 1473-1483.

Moustafa, A. R., Saoudi, A., Moubasher, A., Ibrahim, I. M., Molokhia, H., Schwartz, B., 2003. Structural setting and tectonic evolution of the Bahariya Depression, Western Desert, Egypt. GeoArabia 8, Number 1, Gulf Petrolink, Bahrain.

Mücke, A., Farshad, F., 2005. Whole-rock and mineralogical composition of Phanerozoic ooidal ironstones: comparison and differentiation of types and subtypes. Ore Geology Reviews 26, 227–262.

Parentaeu, M. N., Cady, S. L., 2010. Microbial biosignatures in iron-mineralized phototrophic mats at chocolate pots hot springs, yellowstone national park, united states. Palaios, 25/2, 97-111

Petránek, J., Van Houten, F. B., 1997. Phanerozoic ooidal ironstones. Czech Geological Survey Special paper 7, 71 p.

Préat, A., Mamet, B., De Ridder, C., Boulvain, F., Gillan, D., 2000. Iron bacterial and fungal mats, Bajocian stratotype (Mid-Jurassic, northern Normandy, France). Sedimentary Geology 137, 107-126.

Raiswell, R., 2011. Iron transport from the continents to the open ocean: The aging-rejuvenation cycle. Elements 7, 101-106.

Schwarz, T. and Germann, K. 1993. Ferricrete as a source of continental oolitic ironstones in northern Sudan. Chemical Geology 107, 259-265.

Schwertmann, U., Stanjek, H., Becher, H-H., 2004. Long-term *in vitro* transformation of 2-line ferrihydrite to goethite/ hematite at 4, 10, 15 and 25° C. Clay Minerals 39, 433-438

Sehim, A. A., 1993. Cretaceous tectonics in Egypt. Egyptian Journal of Geology 37/1, 335-372.

Shippers, A., Jørgensen, B. B., 2001. Oxidation of pyrite and iron sulphide by manganese dioxide in marine sediments. Geochimica et Cosmochimica Acta 65, 915-922.

Siehl, A., Thein, J., 1989. Minette-type ironstones. In: Young, T. P., Taylor, W. E. G., (Eds.), Phanerozoic Ironstones. Geological Society Special Publications London 46, 175-193.

Singh, B., Wilson, M. J., Mchardy, M. J., Fraser, A. R., Merrington, G., 1999. Mineralogy and chemistry of ochre sediments from an acid mine drainage near a disused mine in Cornwall, UK. Clay Minerals 34, 301-317.

Sturesson, U., 2003. Lower Paleozoic iron oolites and volcanism from a Baltoscandian perspective. Sedimentary Geology 159, 241-256.

Sturesson, U., Dronov, A., Saadre, T., 1999. Lower Ordovician iron ooids and associated oolitic clays in Russia and Estonia: a clue to the origin of iron oolites?. Sedimentary Geology 123, 63-80.

Sturesson, U, Keikoop, J. M., Risk, M. J., 2000. Modern and Paleozoic iron ooids- a similar volcanic origin. Sedimentary Geology 136, 137-146.

Taylor, K. G., Macquaker, J. S. H., 2011. Iron minerals in marine sediments record chemical environments. Elements 7, 113-118.

Taylor, S. R., McLennan, S.M., 1985. The continental crust: Its composition and evolution. Blackwell, Oxford, 312 p.

Trescases, J.J., 1992. Chemical weathering. In Butt, C. R. M., Zeegers, H., (Eds.), Regolith exploration geochemistry in tropical and subtropical terrains. Elsevier, Amsterdam, 25-40.

Tribovillard, N., Algeo, T. J., Lyons, T., Riboulleau, A., 2006. Trace metals as paleoredox and paleoproductivity proxies: An update. Chemical Geology 232, 12-32.

Van Houten, F. B., 1992. Review of Cenozoic ooidal ironstones. Sedimentary Geology 78, 101-110.

Waychunas, G. A., Kim, C. S., Banfield, J. F., 2005. Nanoparticulate iron oxide minerals in soils and sediments: unique properties and contaminant scavenging mechanisms. Journal of Nanoparticle Research 7, 409-433.

Wedepohl, H., 1995. The composition of the continental crust. Geochimica et Cosmochimica Acta 59, 1217-1239.

Young, T. P., Taylor, W. E. G., 1989. Phanerozoic ironstones, Special publication 46, 251, London, Geological Society.

FIGURE CAPTIONS

Figure 1. A. Geological map of El Bahariya Depression showing the distribution of the main geological units (modified after Hermina et al., 1989, detailed structural elements are shown in Sehim, 1993). B. Location map of the iron ore mine areas.

Figure 2. An outcrop showing the complete stratigraphic succession of the Middle Eocene ironstones in the southern sector of Gabal Ghorabi mine area. A. The lower and upper ironstone sequences consist mainly of four marine ironstone facies; the lower sequence consists of manganiferous mud-ironstone facies, storm-related fossiliferous ironstone facies and nummulitic-ooidal-oncoidal (Nm-Oo-On) ironstone facies. The upper ironstone sequence consists mainly of a lateritic iron ore. B. Close-up view in the upper part of the mud ironstone (paleosol). C. Polished slab shows the nummulitic-ooidal-oncoidal ironstone facies. D. Close-up view shows the paleosol capping the upper part of the nummulitic-ooidal-oncoidal ironstone facies.

Figure 3. Thin section, BSE image and SEM photomicrographs showing the manganiferous mud-ironstone facies. A. An optical photomicrograph showing the ellipsoidal hematite (H) aggregates surrounded by rims of yellow amorphous iron oxyhydroxides, (PPL). B. BSE image showing the growth of pore-filling authigenic clay (C) and manganese (M) minerals. C. A SEM micrograph showing authigenic kaolinite booklets (K) and illite flakes (I) and D. A SEM micrograph showing authigenic todorokite (T). PPL.= plane polarized light, BSE= backscattered electron image and SEM= Scanning electron photomicrograph.

Figure 4. Raman spectra of the various manganese minerals of the different ironstone facies. The lower curves are the measured analyses, while the upper curves are the reference analyses (Ciobota et al., 2011).

Figure 5. X-ray diffraction charts of mud-ironstone (Gh2) and stromatolitic ironstone facies (Gh4) and the lateritic iron ore (Gh17).

Figure 6. Thin sections and SEM photomicrographs of the microbially mediated ironstone facies. A. An optical photomicrograph showing stromatolite columns. B. An optical photomicrograph showing the ferruginous ooids surrounded by quartz cement (Q), (PPL). C &D. SEM photomicrographs showing the spherical and rod-like nanocrystalline iron oxyhydroxides (C) and their diagenetic transformation into microcrystalline goethite (D). E. A SEM photomicrograph showing mat-like microbial laminae overcrowded with cyanobacterial filaments. F. A SEM photomicrograph showing cocci- and bacilli-like bacterial forms are encrusted by nanocrystalline iron oxyhydroxides.

Figure 7. Raman spectra of the different organic materials associated with the iron ooids and oncoids. The lower curves are the measured analyses, while the upper curves are the reference analyses. The measuring parameters include wavelength= 532 nm, obj. 100x, t= 60-180 s, P= 50-500 mW (Ciobota et al., 2011).

Figure 8. Apatite morphology, occurrence and chemistry. A SEM photomicrograph showing the authigenic apatite crystals. B. BSE image showing that the authigenic apatite crystals

are restricted to the cortical laminae of the ferruginous ooids. C. EDAX analysis of authigenic carbonate fluorapatite. D. Raman spectra of the apatite and goethite. The measuring parameters include wavelength= 532 nm, obj. 100x, t= 60-180 s, P= 50-500 mW (Ciobota et al., 2011).

Figure 9. Thin section, BSE image and SEM photomicrographs showing the secondary corrosive $FeSO_4$ and psilomelane laminae. A. An optical photomicrograph showing the secondary corrosive green-colored ferrous iron sulfate laminae, original corroded yellow-colored iron oxyhydroxide laminae and the black-colored psilomelane laminae, (PPL). B. A BSE image showing secondary concordant (parallel) and discordant (cross-cutting) psilomelane laminae inside the cortices of the oncoids and ooids. C & D. SEM photomicrographs showing interlocked plate-like (C) and fibrous (D) psilomelane morphologies.

Figure 10. Thin sections and SEM photomicrograph showing dissolution and reprecipitation features associated with surface and subsurface alteration processes. A. An optical photomicrograph showing the colloform goethite (G) and hematite (H) of the lateritic iron ore type, (PPL). B. A SEM photomicrograph showing the development of cavity-filling botryoidal goethite (G). C. An optical photomicrograph showing development of tabular goethite in a dissolution cavity, (PPL). D. An optical photomicrograph showing the dissolution and fragmentation of the original iron oxyhydroxide laminae by the green-colored ferrous iron sulfates, (PPL).

Figure 11. Enrichment factors of the different ironstone types based on the ICP-MS and ICP-OES analyses. A. Manganiferous mud-ironstone facies (n=4). B. Ooidal-oncoidal-nummulitic ironstone (n=6). C. Ooidal-oncoidal-nummulitic ironstone with hematite and Mn-rich cement (n=2). D. The lateritic iron ore (n=10). E. El Harra paleosol (n=3). n = the number of the analyzed samples.

Figure 12. Laser ablation ICP-MS analyses of one profile passing through one Fe oncoid and the surrounding matrix and silica cement. It shows a positive correlation of P, V, Cr, Zn, As, Mo, Ni and K with iron.

Figure 13. Laser ablation ICP-MS analyses of one profile passing through one Fe oncoid and the surrounding matrix and silica cement. It shows a positive correlation of Ba, Co and Pb elements with manganese.

Figure 14. Chondrite normalized REE pattern of both ooidal-oncoidal ironstone facies (mean = 6) and the lateritic iron ore (mean = 7). B. loss/gain in both facies showing enrichment of the lateritic iron ore in LREEs relative the ooidal-oncoidal ironstone facies.

Figure 15. Back-scattered image of the ooid cortical laminae and element maps show the distribution of Fe, Si, Al, Mn, Ba and K inside of ooidal cortex. Scale bar is 200μm.

Figure 16. X-ray photoelectron spectroscopic analysis of the green laminae. A. X-ray photoelectron spectroscopic survey of the green $FeSO_4$ laminae. B. High-resolution of the Fe $2p_{3/2}$ peak. The Auger electrons, a consequence of photoelectron emission, are not used for this study.

Table CAPTIONS

Table 1. Whole-rock XRF (wt%) and ICP-MS (µg/g) analyses of the manganiferous mud-ironstone and microbially mediated ironstone types.

Table 2. Whole-rock XRF (wt%) and ICP-MS (µg/g) analyses of the lateritic iron ores and paleosols.

Table 3. Selected EPMA data (wt.%) of goethite and hematite of the different iron ore types.

Table 4. Selected EPMA data (wt.%) of psilomelane and todorokite.
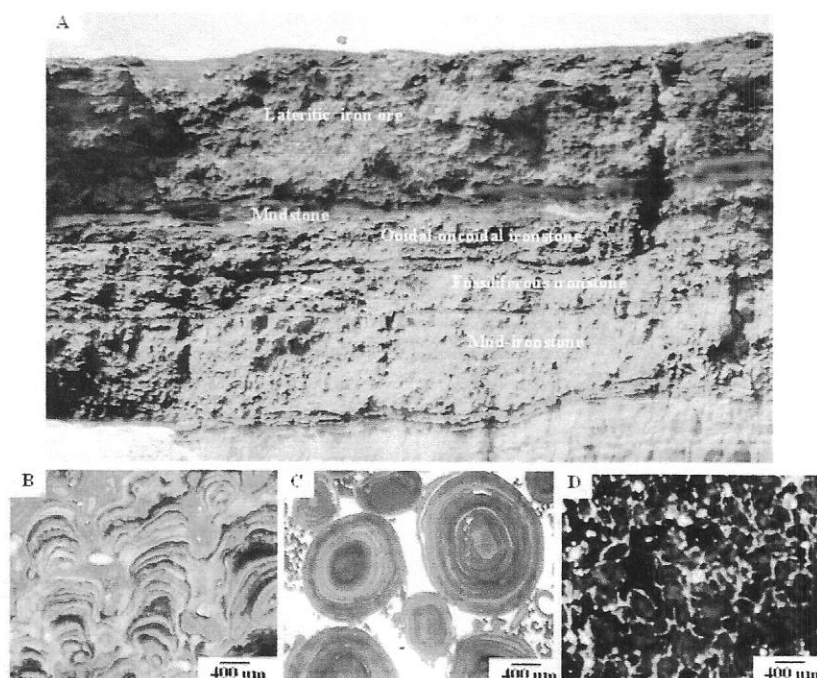
GRAPHICAL ABSTRACT

Research highlights

- We investigate two shallow marine ooidal-oncoidal ironstone sequences
- These sequences were modified by subaerial weathering and subsurface alteration processes.
- The mineralogical composition and geochemical characteristics were examined.
- Iron and manganese oxyhydroxides and oxides are the main constituents.
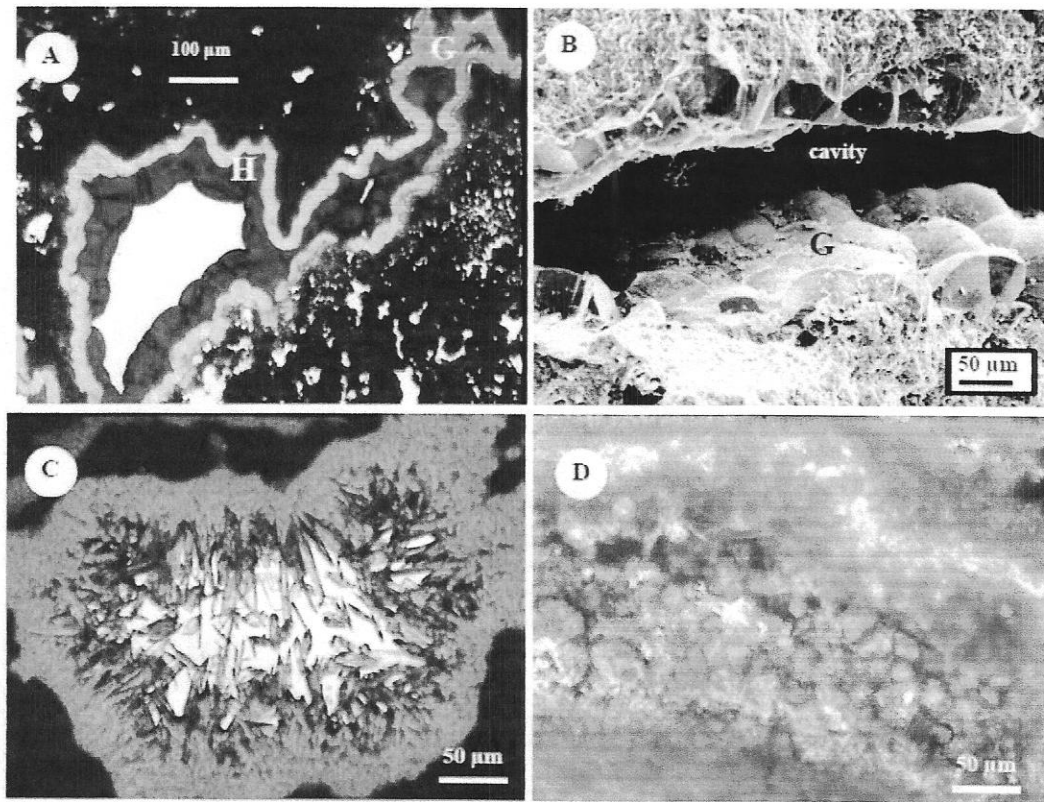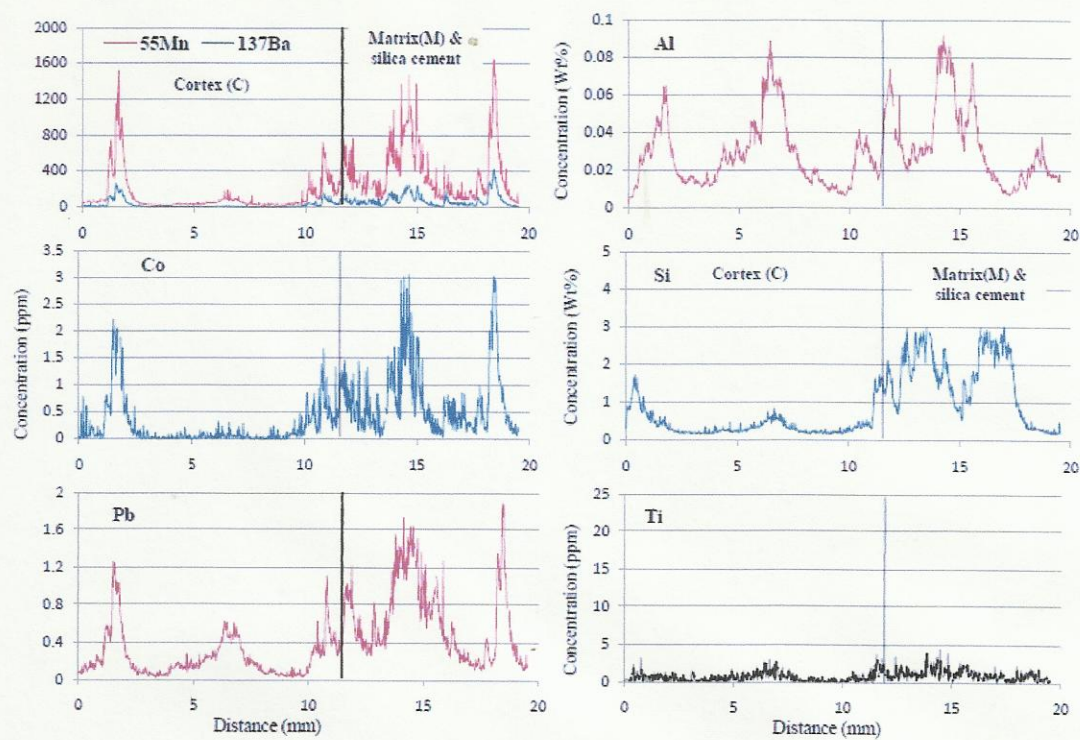- Sulfate, silicate, phosphate and nitrate minerals and organic matter were detected.

Figure 1

Figure 2

Figure 3

Figure 4

wavelength= 532 nm, obj. 100x, t= 60-100 s, P= 1 mW.

wavelength= 532 nm, obj. 100x, t= 60-180 s, P= 50-500 mW.

wavelength= 532 nm, obj. 100x, t= 20 s, P= 5 mW.

Figure 5

G = goethite
H = hematite
Q = quartz
K = kaolinite
Ha = halite
Ca = calcite

38

Figure 6

Figure 7

Carbohydrates

Protein

Organic pigment

Lipids

40

Figure 8

Figure 9

Panel A labels: Psilomelane laminae; Green-colored FeSO₄ laminae; corrosion; Yellow-colored iron oxyhydroxide laminae; scale bar 100 μm

Panel B: scale bar 300 μm

Panel C: scale bar 20 μm

Panel D: scale bar 10 μm

42

Figure 10

Figure 11

Figure 12
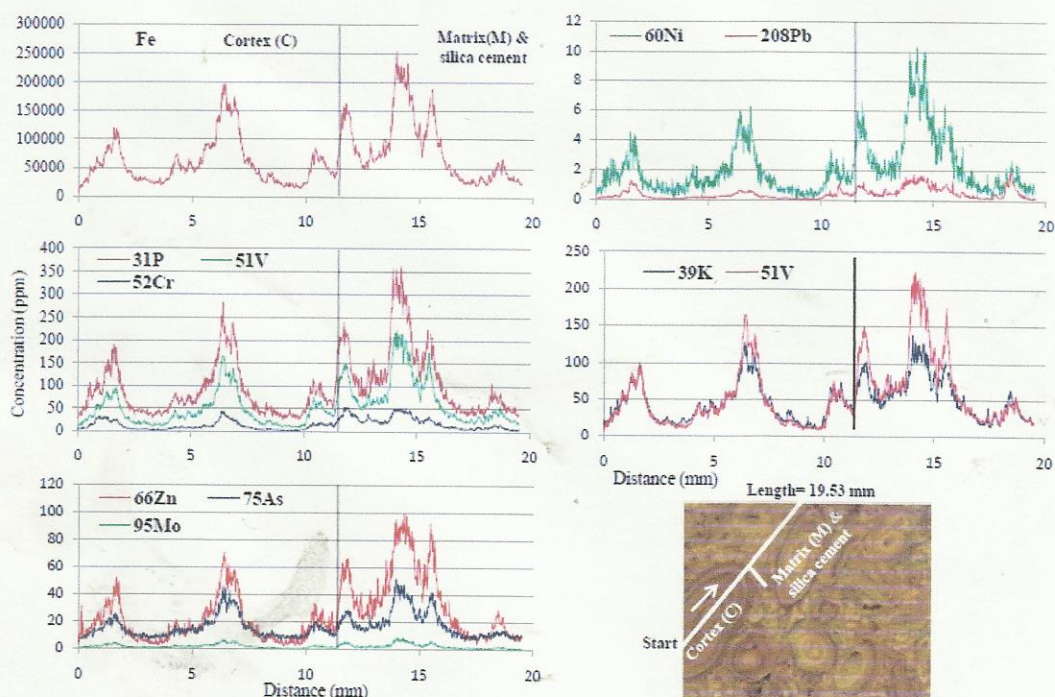
Figure 13

Figure 14

Figure 15

Figure 16